



Optimization and evaluation of oxygen-plasma-modified, aligned, poly (ε-caprolactone) and silk fibroin nanofibrous scaffold for corneal stromal regeneration

Promita Bhattacharjee^{a,b}, Peter W. Madden^{a,b}, Enzo Patriarca^b, Mark Ahearne^{a,b,*}

^a Trinity Centre for Biomedical Engineering, Trinity Biomedical Sciences Institute, Trinity College Dublin, University of Dublin, Dublin, Ireland

^b Department of Mechanical, Manufacturing and Biomedical Engineering, School of Engineering, Trinity College Dublin, University of Dublin, Dublin, Ireland

ARTICLE INFO

Keywords:

Silk fibroin
Stromal regeneration
Oxygen-plasma surface modification
Nanofibre

ABSTRACT

The shortage of human donor corneas for transplantation necessitates the exploration of tissue engineering approaches to develop corneal substitutes. However, these substitutes must possess the necessary strength, transparency, and ability to regulate cell behaviour before they can be used in patients. In this study, we investigated the effectiveness of an oxygen plasma surface-modified poly-ε-caprolactone (PCL) combined with silk fibroin (SF) nanofibrous scaffold for corneal stromal regeneration. To fabricate the electrospun scaffolds, PCL and SF blends were used on a rotating mandrel. The optimization of the blend aimed to replicate the structural and functional properties of the human cornea, focusing on nanofibre alignment, mechanical characteristics, and *in vitro* cytocompatibility with human corneal stromal keratocytes. Surface modification of the scaffold resulted in improved transparency and enhanced cell interaction. Based on the evaluation, a composite nanofibrous scaffold with a 1:1 blend of PCL and SF was selected for a more comprehensive analysis. The biological response of keratocytes to the scaffold was assessed through cellular adhesion, proliferation, cytoskeletal organization, gene expression, and immunocytochemical staining. The scaffold facilitated the adhesion of corneal stromal cells, supporting cell proliferation, maintaining normal cytoskeletal organization, and promoting increased expression of genes associated with healthy corneal stromal keratocytes. These findings highlight the potential of a surface-modified PCL/SF blend (1:1) as a promising scaffolding material for corneal stromal regeneration. The developed scaffold not only demonstrated favourable biological interactions with corneal stromal cells but also exhibited characteristics aligned with the requirements for successful corneal tissue engineering. Further research and refinement of these constructs could lead to significant advancements in addressing the shortage of corneas for transplantation, ultimately improving the treatment outcomes for patients in need.

1. Introduction

The cornea is the transparent layer of the anterior eye, responsible for focussing light. The major structural unit of the cornea is the stroma, consisting of about 90% of corneal thickness. It comprises of collagen fibrils with normally quiescent keratocytes in a collagen/proteoglycan matrix [1,2]. These fibrils are aligned in a highly ordered network of lamellae, and the structured architecture and composition maintains not only mechanical strength and corneal shape, but also corneal transparency [3,4]. If there is disruption of this stromal architecture due to damage from disease or injury, then corneal opacity and ultimately blindness results [5]. To restore sight in this case, transplantation

(keratoplasty) of the cornea from a deceased donor is a widely adopted treatment. Unfortunately, a shortage of human donor corneas limits the number of treatments that can be performed [6]. To address this shortage, a tissue engineering approach has been investigated [7], to develop non-human biomaterials to substitute for human donor tissue.

Acellular scaffolds fabricated from decellularized animal stromal tissue have been used to replicate human corneal scaffold architecture [7,8]. However, a synthetic construct, or one where the constituents can be recombinant or processed and highly purified, can reduce the risk of infectious agents, contamination, provide consistent quality and avoid the need for one donor eye for every transplant eye. The most abundant protein present in the human cornea is collagen type I. For this reason,

* Corresponding author at: Trinity Centre for Biomedical Engineering, Trinity Biomedical Sciences Institute, Trinity College Dublin, University of Dublin, Dublin, Ireland.

E-mail address: ahearnm@tcd.ie (M. Ahearne).

<https://doi.org/10.1016/j.bbiosy.2023.100083>

Received 2 June 2023; Received in revised form 28 August 2023; Accepted 2 September 2023

Available online 3 September 2023

2666-5344/© 2023 The Authors. Published by Elsevier Ltd. This is an open access article under the CC BY-NC-ND license (<http://creativecommons.org/licenses/by-nc-nd/4.0/>).

highly purified or recombinant collagen has been widely examined for corneal regeneration [9,10]. This usually involves the production of collagen fibres as a scaffold onto which corneal keratocytes can attach and grow. Unfortunately, despite such constructs potentially having the necessary transparency and ability to support the active migration of keratocytes, many of these constructs have inferior mechanical strength and stiffness when compared to native tissue [11,12]. Furthermore, the mechanical properties of scaffolds fabricated solely with collagen do not restrict keratocyte phenotype to the normal quiescent state [13]. Keratocyte normality is vital to secrete proteoglycans and various collagen subtypes to form a normal corneal extracellular matrix (ECM), which is also important to ensure transparency, nerve growth and cell adhesion [14,15]. However, trying to repopulate these scaffolds with cells is difficult and so hydrogels formulated from decellularized corneal ECM have also been investigated [16,17]. Cell seeded ECM-derived hydrogels showed elevated expression of keratocyte associated markers when compared to cells in collagen hydrogels [17]. However, these ECM-derived hydrogels did not achieve the aligned fibril structure or mechanical strength observed in stroma. Several other studies have investigated different biomaterial-based systems for use in corneal stromal regeneration [18,19].

Electrospinning is an effective approach to manufacture nanofibrous scaffolds that can mimic native tissue characteristics [20,21] and improve the mechanical properties of corneal constructs. Poly- ϵ -caprolactone (PCL) is a synthetic polymer that has been widely investigated for biomedical application due to its stability, capability to form nanofibres and cytocompatibility [22]. PCL nano-capsules and nanoparticles have been investigated as a long-term glaucoma treatment [23] as well as an enhanced treatment for macular degeneration [24]. In spite of these advantages, a limitation with PCL is that it is hydrophobic, which hinders cell adhesion [25]. Surface modification of PCL has been employed to address this problem and this can increase hydrophilicity, improving not only cell attachment, but also cell growth and proliferation [26], without altering the inherent scaffold characteristics. Various surface modification methods have included, end-grafting, γ -ray irradiation, plasma treatment, and laser induced ozone oxidization [27–31]. Of these, plasma treatment is an inexpensive and ecologically sound method [32] that generates electrochemically active species on the surface, which react with environmental oxygen to form hydrophilic functional groups without the need for chemical catalysts that can leave behind toxic residues. Additional improvement regarding cellular adhesion and cytocompatibility has been reported for composite nanofibrous scaffolds developed by electrospinning blends of PCL with other natural biopolymers [33].

In the current study to develop a bioengineered cornea, a combination of PCL and natural silk fibroin (SF) was chosen. SF is a promising polymer for biomedical applications because of its non-human origin, mechanical strength, cytocompatibility, tuneable biodegradability and capacity to stabilize labile compounds [34–36]. SF can also be manufactured transparent, which is crucial for use in the ocular pathway [37–41]. Silk sutures have regulatory approval from US Pharmacopeia, as do commercially available surgical scaffolds (SERI scaffolds, Allergan, USA), using silk fibroin, for abdominal wall repair. Furthermore, fibroin has undergone clinical trials for tympanic membrane and breast reconstruction, with three devices already approved for clinical use [42].

The aim of this study was to evaluate a non-mammalian corneal stromal scaffold fabricated by electrospinning aligned nanofibres, using different ratios of PCL and SF. The influence of the blending ratio and plasma treatment was investigated. Based on this information, a scaffold was selected for in-depth evaluation to determine optimal fabrication conditions. This showed that such a plasma treated PCL/SF nanofibrous scaffold supported a normal keratocyte phenotype.

2. Materials and methods

Unless otherwise stated, reagents and chemicals were bought from Sigma-Aldrich.

2.1. Preparation of base solutions for electrospinning

A 10 % wt/wt solution of PCL (Mol. wt.=80,000) in chloroform was prepared by continuous stirring for 3 h at 37°C. Following a previously established protocol, SF from *Bombyx mori* cocoons (Treenway silks, USA) was extracted [43].

2.2. Fabrication of nanofibrous scaffolds

PCL and SF combinations (Supplementary Table 1) were made just prior to use, by volume ratio and gentle stirring for 15 min at ambient temperature [44]. Electrospinning nanofibrous scaffolds using 4wt% and 6wt% concentrations of SF alone does not yield viable scaffolds and PCL blends allow a greater control over the material properties and potential applications. To fabricate a nanofibrous scaffold, the blended solution was drawn into a 10 mL glass syringe and a blunt-ended needle attached (22G, inner diameter 0.413 mm). A plastic sleeve was used to electrically isolate mounting the syringe onto a syringe pump (NE-1000 Programmable Single Syringe Pump, KF Technology). Dispersion was fixed at a rate of 0.5 mL per hour. To align the fibres, a rotating mandrel collector, covered with aluminium foil, was placed 15 cm from the needle tip. Mandrel rotation speed was 2,500 rpm and a voltage of 11 kV was applied between the needle and the grounded collector, using a high-voltage power supply (G25 high voltage power supply, Gigavac). After electrospinning for 5 h, the fibre sheet scaffold was dried under vacuum (50 mbar, 25°C) for 72 hours. After drying, scaffolds were treated (100% EtOH for 5 min, then 70% EtOH for 20 min) to cause β -sheet formation of SF [43]. They were stored dry in a desiccator until use.

In the setup with a rotating collector, mechanical forces are employed to pull the fibre while depositing it on a spinning drum, thus inducing fibre alignment [45]. At low speeds, the mandrel's rotation is inadequate to affect the bending instability, leading to the deposition of random fibres. However, as the rotational velocity of the mandrel increases, so does the mechanical drawing force, resulting in a proportional enhancement of fibre alignment. The most significant alignment occurs when the rotational velocity of the collector is balanced or surpasses the ejection rate of the fibre, whilst still ensuring it does not break.

2.3. Surface modification of fabricated composite nanofibrous scaffolds

A low-pressure glow plasma reactor (PICO, Diener, Germany) was used to conduct plasma treatment on fabricated nanofibrous scaffolds. The scaffold was held between two rectangular aluminium plate electrodes at 15 kHz and 3.5 kV, covered with glass dielectric sheets. A 3:1 ratio of helium and oxygen was passed between the electrodes. The resulting glow plasma was optimized to 20 min duration. The treated scaffolds were then washed in deionized (DI) water for 3 h to remove by-products and were stored in a vacuum desiccator before use.

2.4. Characterization of fabricated nanofibrous scaffolds

2.4.1. Physical, optical, chemical and mechanical characterizations

Nanofibrous scaffold morphology was analysed by scanning electron microscopy (SEM, EVO 60, Carl Zeiss, Germany). Fibre diameter was determined using Image J (Fiji) [46]. The fibre diameter was quantified at 40 arbitrary sites on the SEM image frame. The values were averaged to obtain the representative value.

To assess hydrophobicity, advancing and receding contact angles of fabricated scaffolds with respect to water were measured using an

optical goniometer (Data Physics Instruments, Filderstadt, Germany).

The fabricated scaffolds need to exhibit optical characteristics comparable to a healthy cornea to serve as a suitable substitute. For this reason, scaffolds were tested for light transmission before and after surface modification. The scaffolds were submerged in phosphate-buffered saline (PBS) using a 12-well plate (Bio-one, Greiner). Scaffold light transmission was measured across the visible light spectrum of 400 nm to 750 nm wavelength using a microplate reader (Synergy HTX, BioTek) after subtracting the base value of a well with PBS alone. An average of three measurements was made. Refractive index was evaluated using a refractometer (Optilab T-rEX, Wyatt Technology, USA). Attenuated total reflectance-Fourier transform infrared (ATR-FTIR, Nexus-870, Thermo Nicolet Corporation, USA) was conducted to examine the chemical composition of the scaffolds, with a 4% SF solution as a control. Under ambient conditions, the spectra were recorded over a range of 2500–500 cm^{-1} .

To obtain the Young's modulus of the fabricated nanofibrous scaffolds, samples were cut into a dumbbell shape (50 mm long, 10 mm wide), then rehydrated with PBS for 72 h. Tensile measurements were performed (E1000 UTM; Instron) at 25°C and 50% relative humidity with a 200 N load-cell and a 3 mm/min extension rate. Young's modulus was calculated from the linear region of the stress-strain curves.

2.4.2. Cell isolation and culture

Following the previously established protocol, human corneal keratocytes were isolated from donor tissue in accordance with the Declaration of Helsinki [47] and with ethics approval from Trinity School of Medicine Ethics Committee. These primary cells were cultured in media comprising of Dulbecco's Low Glucose Modified Eagles Medium (DMEM) (Hyclone; Thermo Fisher Scientific) supplemented with 10% fetal calf serum (Hyclone) and 1% penicillin/streptomycin in a controlled, humidified environment of 5% CO_2 , at 37°C. Cells at passage 3 were used for the experiments. At this time subsequent media was changed to serum-free, consisting of DMEM/F12 (Hyclone; Thermo Fisher Scientific), supplemented with 1% penicillin/streptomycin, 100 $\mu\text{g}/\text{mL}$ L-ascorbic acid and 1 $\mu\text{L}/\text{mL}$ Insulin-Transferrin-Selenium (100 \times , Gibco). The use of serum-free media has been shown to better maintain a quiescent keratocyte morphology [48].

To decontaminate the nanofibrous scaffold, 1 cm^2 samples were treated with 70% ethanol, followed by a 20 min exposure to UV inside cell culture hood. Scaffolds were then washed three times with sterile PBS over 20 min, followed by soaking in the serum-free culture medium for 4 h to prime the scaffold to support cell attachment. The scaffolds were then removed from the medium and allowed to partially dry for 1 h in the cell culture cabinet. 20mL of cell suspension in media, containing 1000 cells, was seeded onto each nanofibrous scaffold and, to allow cell adhesion, the scaffolds were kept at 37°C and 5% CO_2 in a humidified environment for one hour. Scaffolds were then rinsed in PBS to remove unattached cells and the scaffold returned to cell culture. Cell seeded scaffolds were cultured using the serum-free media for up to 21 days. Media was replaced every alternate day.

2.4.3. Evaluation of cellular metabolic activity

An MTT assay was performed in accordance with the manufacturer's protocol (M5655, Sigma) at different time points over the culture period to evaluate the cellular toxicity of the fabricated scaffolds.

2.5. Detailed evaluation on selected nanofibrous scaffolds

The nanofibrous scaffold found to have the highest cell growth and proliferation was selected for further studies of thermogravimetric analysis of molecular structure, biophysical measurement of fibre swelling, *in vitro* biodegradation characteristics and a detailed cyto-compatibility analysis. Following the growth of cells on the scaffold, we investigated if these cells would begin to behave like native corneal stromal keratocytes. In these studies, nanofibrous scaffold fabricated

from PCL alone served as control.

2.5.1. Thermogravimetric analysis

Thermogravimetric Analysis (TGA) was performed (Pyris Diamond TG-DTA thermo-gravimetric analyser, Perkin Elmer) from ambient temperature to 900°C, at 10°C /min, in synthetic air (80% N_2 , 20% O_2).

2.5.2. Swelling ratio

The swelling of the scaffolds was evaluated by placing the dry scaffold into PBS at 37°C. For each group, triplicate samples were removed at set time points, blotted dry, and then weighed. The samples were then promptly returned to the PBS and the process repeated. The following Eq. (1) was used to quantify the swelling ratio

$$\text{Swelling ratio}(\%) = \frac{W_s - W_o}{W_o} \times 100 \quad (1)$$

Where W_o = the initial dry weight of the sample and W_s = the weight of the sample after a specific time point.

2.5.3. Enzymatic degradation

An enzymatic degradation study was carried out with proteinase K from *Tritirachium album* [49]. 0.5 $\text{cm} \times 0.5 \text{ cm}$ nanofibrous scaffolds were incubated at 37°C in 2 mL PBS as control or Proteinase K (2 $\mu\text{g}/\text{mL}$) in PBS on a rotary mixer at 100 rpm. Solutions were replaced on alternate days. The scaffold was removed on day 1, 7, 14 and 21, blotted to remove excess liquid, and weighed to measure the extent of enzymatic degradation, before being replaced.

2.5.4. Evaluation of cellular adhesion, proliferation and toxicity

A 20 μL human corneal keratocytes cell suspension, containing 1000 cells, was seeded onto the scaffolds. Cell adhesion was quantified by changing the media after 1, 3 and 5 h of seeding and measuring the density of cells in the extracted media [50]. The number of cells remaining on the scaffold was taken as the difference between the seeding inoculation count and the extracted media count, without any consideration of cell death or proliferation.

Cell metabolic activity was assessed using a PrestoBlue assay (Molecular Probes; Invitrogen, Carlsbad, CA) over the 21 days of culture period. Metabolic activity by this assay was taken to be a measure of cell proliferation.

Cell viability was accessed by a calcein cell membrane permeability assay (Molecular Probes, USA) after 5 days of culture. Live cells were stained with calcein (green coloration; excitation: 488 nm) and dead cells with ethidium homodimer (red coloration; excitation: 543 nm). Confocal microscopy (Leica SP8, Leica) was used to examine the cell staining.

2.5.5. Cellular morphology within the construct

To examine the cytoskeletal organisation of seeded cells after 10 days of culture, cell-laden constructs were first fixed with 4% paraformaldehyde for 15 min. They were then treated with 0.1% Triton X-100 solution in 1% bovine serum albumin (BSA) to permeabilize the cells, and then incubated with 2% BSA for 1 hour to block non-specific antigens. Phalloidin-TRITC was used to stain actin filaments (F-actin) for 1 h, using the manufacturer's protocol. Following washing, the constructs then received a second stain with 4',6'-diamidino-2-phenylindole (DAPI, 1 mg/mL , 1:500 dilution) to highlight cell nuclei. A Leica SP8 confocal microscope was used to view cytoskeletal organisation and LAS X Advanced software used for image processing.

For SEM imaging, cell-seeded scaffolds were fixed using 4% paraformaldehyde and then dehydrated using ethanol gradients (50–100 % v/v; 20 min each), followed by brief exposure to isoamyl alcohol. SEM was carried out using a ZEISS scanning electron microscope after gold coating. A schematic of blended scaffolds with cells was presented in supplementary Fig. 1.

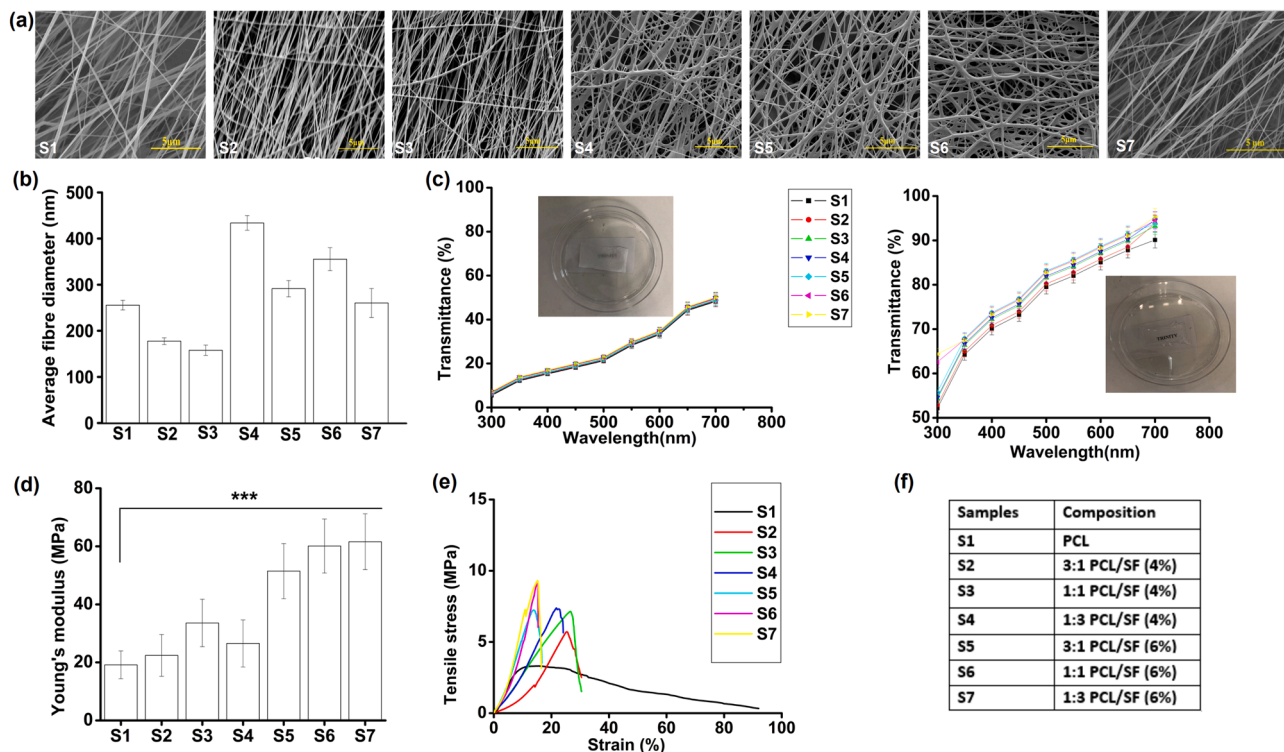


Fig. 1. (a) SEM images of fabricated scaffolds; (b) average fibre diameters within scaffolds; (c) light transmission before and after plasma surface treatment; (d) Young's modulus of scaffolds; (e) stress-strain relationship under tension ($n=3$ for all data shown); (f) composition details of scaffolds.

2.5.6. Immunocytochemistry

After 14 days of culture, samples were fixed, permeabilized and blocked using the same method used to prepared cells for F-actin staining. For immunocytochemical staining, samples were then incubated for 18 h at 4°C in a range of antibodies, anti-ALDH3A1 1:50 (ab76976; Abcam, Cambridge, United Kingdom), anti-keratocan 1:50 (sc-66941; Santa Cruz, Heidelberg, Germany), or anti- α -smooth muscle actin (α SMA) 1:50 (ab7817; Abcam). They were then washed thrice with PBS, 20 min for every wash and then incubated with fluorescently labelled antibodies for 1h at ambient temperature, in the dark. To highlight ALDH3A1 and Keratocan, Donkey anti-rabbit Alexa Fluor 488 (ab150073; Abcam) was used. For α SMA, goat anti-mouse biotin followed by ExtrAvidin-FITC (B7151 and E2761; Sigma). Constructs were washed with PBS and counterstained with DAPI (1 mg/mL, 1:500 dilution) to visualize nuclei. Confocal microscopy was performed on the Leica SP8 with LAS X Advanced software 2.13 post-processing.

2.5.7. Gene expression by rtPCR

Real-time reverse transcription polymerase chain reaction (rtPCR) was conducted to quantify relative gene expression at day 14 and 28, following a previously described protocol [50]. The following primers (Applied Biosystems, Biosciences, Dublin, Ireland) were examined: α SMA (Hs00426835_g1), ALDH3A1 (Hs00964880_m1), collagen type III (COL3A1; Hs00943809_m1), collagen type I (COL1A1; Hs00164004_m1), collagen type V (COL5A1; Hs00609133_m1), decorin (DCN; Hs00754870_s1), glyceraldehyde-3-phosphate dehydrogenase (GAPDH; Hs02758991_g1), keratocan (KERA; Hs00559942_m1), and lumican (LUM; Hs00929860_m1). Gene expressions were normalized against the housekeeping gene, GAPDH and the values represented as the exponential form of $2^{-\Delta\Delta Ct}$.

2.5.8. Biochemical assays

Biochemical analysis of sulphated glycosaminoglycans (sGAG) and DNA was undertaken after 14 and 28 days of culture using a previously described protocol [50]. The cell-loaded scaffolds were first macerated

at 60°C for 16 h in a digestion solution (125 μ g/mL papain, 5 mM L-cysteine, 100 mM Na_2HPO_4 , 5 mM EDTA, pH 6.8). A dimethyl-methylene blue (DMMB) binding assay kit (Blyscan; Biocolor Ltd., Antrim, UK) was then used to measure sGAG. To do this, the DMMB solution was mixed with each sample and absorbance measured at 590 nm using a microplate reader (Synergy HTX, BioTek). Total sGAG was quantified against a standard of bovine chondroitin sulfate. Bisbenzimidazole Hoechst 33258 was used to stain cell nuclei DNA and the quantity of staining was a measure of cell density.

2.6. Statistical analysis

One-way ANOVA was used to compare the results, followed by Tukey's post-hoc HSD test. Significant differences are shown as $***p < 0.001$; $**p < 0.01$; $*p < 0.05$. Unless otherwise specified, 3 samples were used per experiment and presented as mean \pm standard deviation (SD).

3. Results

3.1. Physical and chemical characterization of scaffolds

SEM images of scaffolds are presented in Fig. 1(a) and the average fibre diameter is in Fig. 1(b). No bead formation was found on the SEM images for any of the blends. However, the blending ratio of PCL to SF exhibited a marked influence on fibre diameter, regardless of whether the SF was 4 wt% or 6 wt% (Fig. 1(b)). Fibres were well aligned, and the thinnest fibres were produced for a 1:1 PCL/SF 4% blend ratio.

Before surface modification, the percentage transmission of visible light through the scaffolds was less than 50%, but after plasma treatment transmission was significantly increased to over 90% (Fig. 1(c)). After plasma surface treatment and transfer to water, there was no significant difference of transparency between the groups. The refractive index (RI) of plasma surface-modified scaffolds, regardless of blend, was 1.43 ± 0.14 .

Young's modulus for the scaffolds are presented in Fig. 1(d). The

modulus of the scaffolds increased with increasing SF apart from the 1:3 PCL/SF (4%) composition where the modulus decreased relative to the 1:1 PCL/SF (4%) composition. The tensile strength and elongation at break are shown in Fig. 1(e). All scaffolds were shown to be ductile. Tensile strength increased with increasing SF when 6% SF was used. However, this was not the case with 4% SF where the 1:1 PCL/SF having the greatest tensile strength.

The spectra of PCL/SF blends were assessed to determine if both PCL and SF individual spectra were present, or if a new spectra was formed. The influence of silk fibroin in the fabricated nanofibrous scaffolds was demonstrated by analysis of FTIR spectra (Fig. 2(a–c)). Three distinct vibration peaks that correlate with amide groups of SF were recorded in FTIR spectra; 1,650–1,630 cm^{-1} for amide I (C=O stretching), 1,540–1,520 cm^{-1} for amide-II (secondary NH bending, due to β -sheet structure), and 1,270–1,230 cm^{-1} for amide III (C–N and N–H functionalities). The vibration peaks and the strongest bands recorded for PCL only scaffolds were: 2945 cm^{-1} , asymmetric CH_2 stretching; 2868 cm^{-1} , symmetric CH_2 stretching; 1726 cm^{-1} , carbonyl stretching (C=O); 1251 cm^{-1} , C–O and C–C stretching in the crystalline phase; 1210 cm^{-1} asymmetric C–O–C stretching; 1130 cm^{-1} , C–O and C–C stretching in the amorphous phase.

The PCL/SF blended nanofibrous scaffolds showed peaks associated with both SF and PCL without major variation, although there was a minor peak shift, indicated by the vertical line (Fig. 2b and c). Overall, FTIR spectra of composite nanofibrous scaffolds comprised absorption peaks corresponding to PCL and SF, without any extensive peak shift or transformation. For all blended scaffolds, a few minor absorption peaks were identified in the range of 1700 to 1100 cm^{-1} , indicated by the blue dotted box.

The contact angles of nanofibrous scaffolds were measured before and after surface modification, as presented in Fig. 2d. The results show that surface modification reduced the hydrophobicity of all blends. Such a change would be expected to increase cell adhesion and survival.

3.2. Metabolic activity of cells

Metabolic activity increased through the 21 days for all scaffold compositions, indicating an increase in proliferation. The increase was significantly lower where cells were cultured on scaffold made from just PCL or 3:1 PCL/SF compared to scaffold containing higher ratios of SF ($p < 0.001$) (Fig. 2(e,f)). These results suggest that SF supports better cellular metabolic activity and proliferation. For this reason, 1:1 PCL/SF blends were chosen for thermal, biophysical and more detailed cyto-compatibility analysis.

3.3. TGA, swelling and degradation of scaffolds

Thermal properties of composite scaffolds were analysed with TGA (supplementary Fig. 2(a)). PCL only showed a simple, one-step, degradation profile with a single transition temperature. The degradation profile also demonstrated a higher thermal stability than composite scaffolds. Degradation started at 342°C with complete degradation by 489°C. 1:1 PCL/SF scaffolds started degrading at 282°C (6%SF) and 295°C (4%SF) with full degradation at 506°C (4%SF) and 516°C (6%SF). Thus, the initial onset of degradation decreased with increasing SF concentration. The presence of a two-step degradation in the TGA profile of composite scaffolds indicates that it is formed from two polymers.

Supplementary Fig. 2(b) shows the swelling ratios of nanofibrous scaffolds and the point they reached equilibrium. Blended scaffolds swelled more readily and had a higher swelling ratio (81 % for S3 and 83 % for S6) compared with pure PCL nanofibrous scaffold (52 % for S1).

No marked loss in weight was found in the PCL or PCL:SF blends incubated in control PBS solution (pH 7.4) (supplementary Fig. 2(c)). However, enzymatic treatment over 21 days resulted in ~34.8% loss in dry weight for PCL, ~60.7% for 1:1 PCL/SF (4%) and ~64.8% for 1:1 PCL/SF (4%) (supplementary Fig. 2(d)). The SF blended scaffolds degraded at a faster rate initially, compared with PCL, but the rate slowed after seven days.

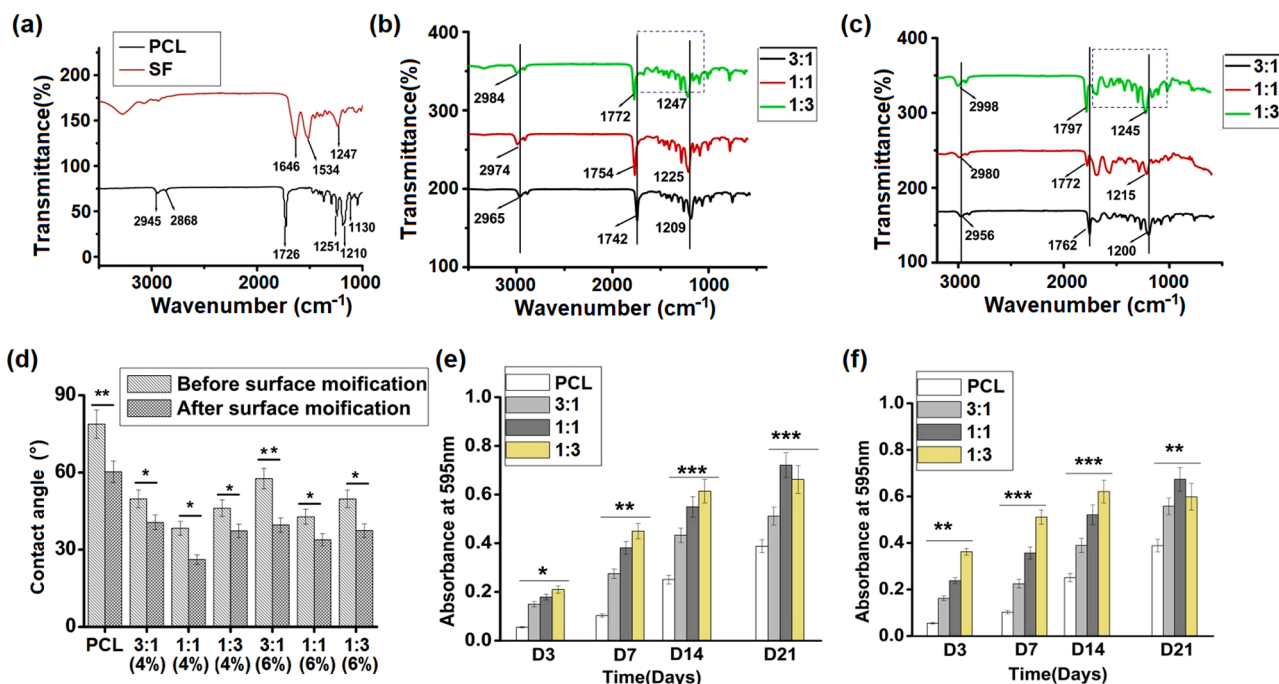


Fig. 2. FTIR spectra of (a) PCL and SF solution; (b) PCL/SF scaffolds fabricated with different blending ratio of PCL and 4wt% SF; (c) PCL/SF scaffolds fabricated different blending ratio of PCL and 6wt% SF. Composite scaffolds reveal peaks corresponding to β sheet structure of SF and respective absorption peaks of PCL without any major alterations. (d) Hydrophilicity PCL and different ratio PCL/SF scaffolds (%SF shown) before and after surface modification. Surface modification significantly increased hydrophilicity of the scaffolds. Total cell metabolic activity on (e) PCL/SF scaffolds fabricated with different blending ratio of PCL and 4 wt% SF and (f) PCL/SF scaffolds fabricated with different blending ratio of PCL and 6 wt% SF. PCL without SF served as a control ($n=3$ for all data shown).

3.4. Cytocompatibility analysis

Keratocytes more promptly attached onto SF blended scaffolds, compared with the PCL only controls (Fig. 3(a)). Within the first hour, 44, 69 and 66 % of cells had attached onto PCL, 1:1 PCL/SF (4%) and 1:1 PCL/SF (6%) scaffolds respectively. These values increased to 67, 94, and 93% over the next four hours. However, after 5 h of seeding there was no significant difference in cellular adhesion between the two PCL/SF groups. Cell proliferation continued, and at day 21 was significantly higher ($p < 0.01$) for PCL/SF scaffolds (S3, S6) as compared with PCL only scaffolds (Fig. 3(b)).

The viability of cells on different nanofibrous scaffolds was examined using a live/dead staining assay (supplementary Fig. 3(a)). Cells cultured on all scaffolds remained viable with no dead cells detected, implying the scaffolds were not cytotoxic. There were more cells present on PCL/SF scaffolds than PCL only scaffolds. As with the results from the proliferation assay, this suggests that the addition of SF to PCL enhances cell proliferation.

The cytoskeletal organisation of cells regulates essential cellular phenomenon like adhesion, and migration. More actin stressed fibres were observed within PCL/SF scaffolds when compared with PCL only scaffolds as shown in supplementary Fig. 3(b). The control PCL scaffold displayed scattered and irregular actin distribution, which appeared restricted to the periphery of the cell. With all scaffolds, actin fibres were mostly aligned along the scaffold fibre direction.

SEM imaging of cell-seeded scaffolds show that the cells on SF blended scaffolds had a flatter profile, formed contiguous, multilayer sheets, and covered more of the substrate compared to the PCL only control (supplementary Fig. 4(a)).

3.5. Characterization of ECM

At day 28, quantification of sGAG on 1:1 PCL/SF (4 and 6%) scaffolds demonstrated significantly ($p < 0.01$) more sGAG compared to PCL only scaffolds (Fig. 3(c)). This was also the case when the sGAG was normalized to the DNA present at day 14 and 28 (Fig. 3(d)).

3.6. Immunofluorescent staining and gene expression

Markers associated with keratocyte and myofibroblastic phenotypes were evaluated by immunofluorescent staining (Fig. 4). Keratocyte markers ALDH3A1 and keratocan were present in cells on all nanofibrous scaffolds. None of the scaffolds showed any detectable levels of α SMA, a myofibrotic marker. Quantification of these images found significantly more ALDH3A1 and keratocan on scaffolds containing SF compared to PCL only, although it was not determined how much of the increased staining was due to changes in the cell phenotype or cell density (supplementary Fig. 4 (b)).

Gene expression of several keratocyte markers was evaluated using rtPCR after 14 and 28 days of culture. Blending with SF significantly increased the expression of ALDH3A1, keratocan, decorin and lumican by day 28 (Fig. 5). ALDH3A1 expression was significantly increased for 1:1 PCL/SF (4% and 6%) (13.1 ± 1.15 and 12.9 ± 1.47 fold increase respectively) when compared with PCL at day 28 (5.63 ± 0.71). A significant increase in keratocan was also demonstrated for 1:1 PCL/SF (4% and 6%) (10.22 ± 1.32 and 10.78 ± 1.05 respectively) compared with PCL (5.26 ± 0.92). Significant increments for lumican and decorin were also recorded for SF blended nanofibrous scaffolds, compared with PCL only scaffolds.

Expression of collagen type I, III and V, the most abundant collagens

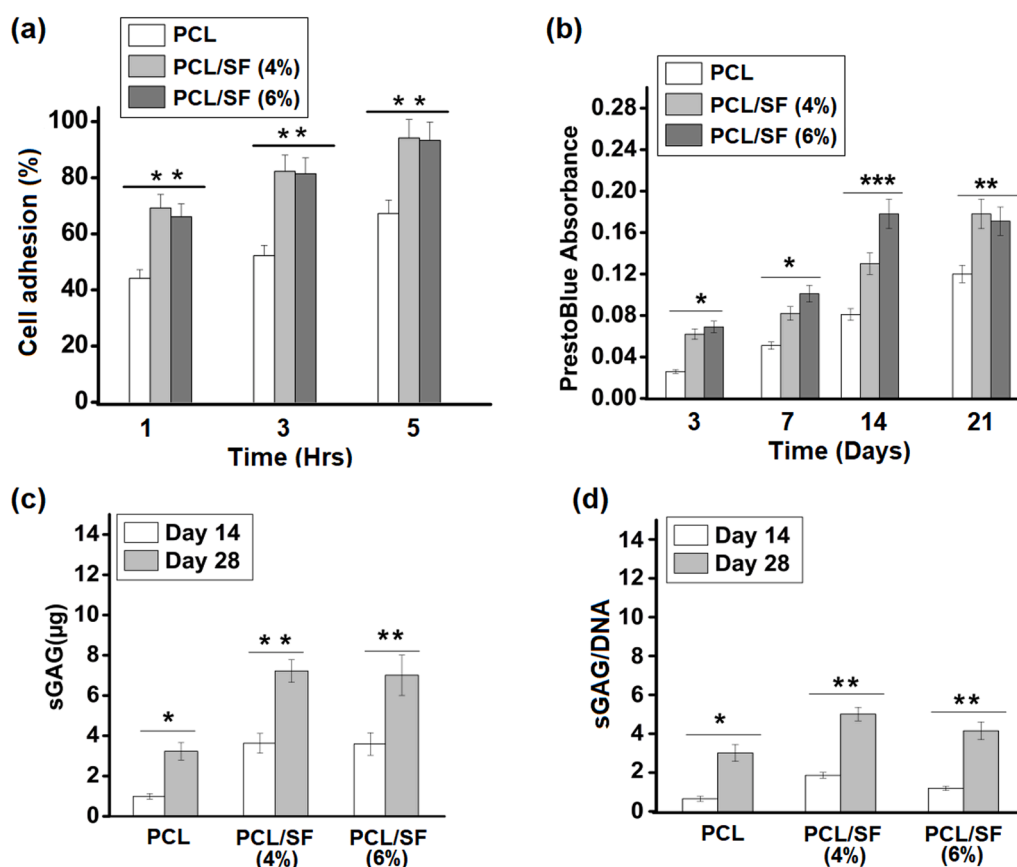


Fig. 3. (a) Initial cell attachment efficiency and (b) measure of cellular proliferation on PCL and 1:1 PCL/SF scaffolds; (c) sGAG production as quantified by DMMB assay; (d) ratio of sGAG/DNA. At day 28, quantification of sGAG on 1:1 PCL/SF (4% and 6%) scaffolds demonstrated significantly ($p < 0.01$) more sGAG compared to PCL only scaffolds. Same trend was recorded when the sGAG was normalized to the DNA present at day 14 and 28 ($n=3$ for all data shown).

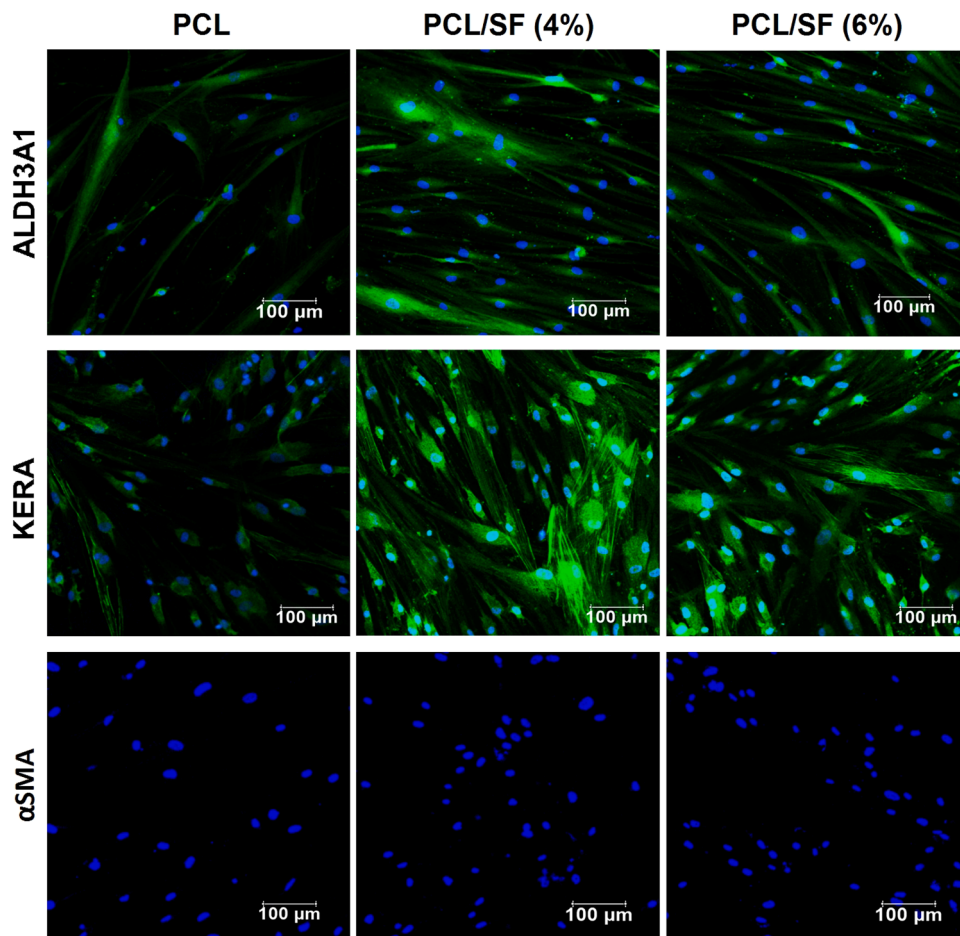


Fig. 4. Immunofluorescent staining of protein markers ALDH3A1, keratocan and αSMA (all green) and nuclei (blue) after 14 days in culture.

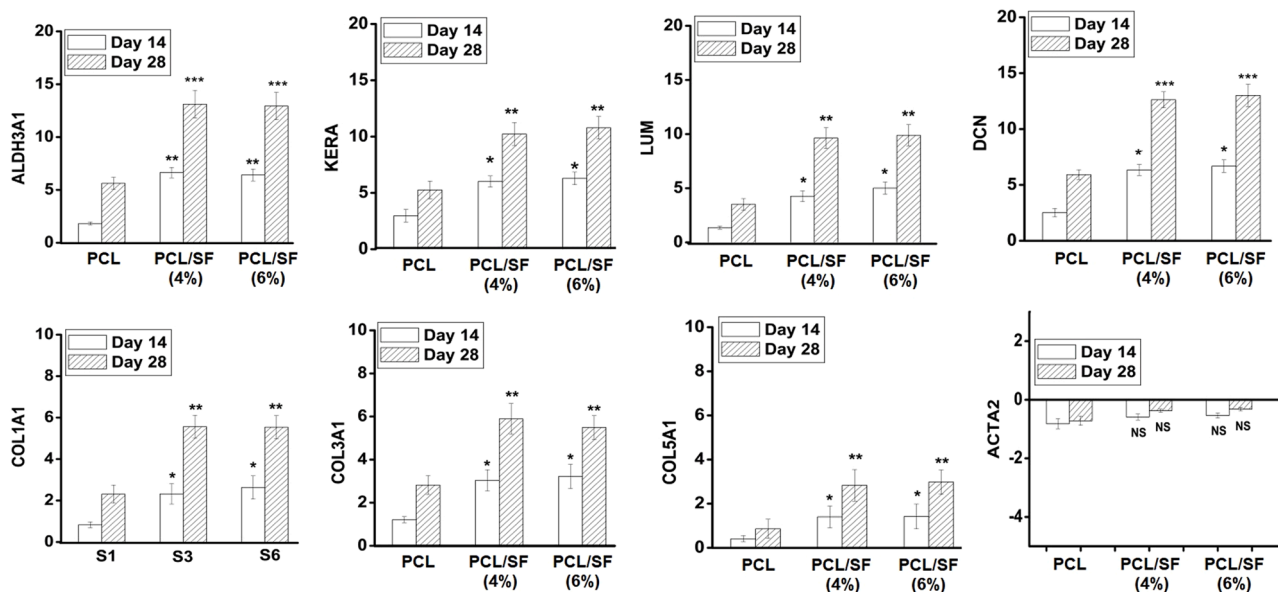


Fig. 5. Fold change gene expression analysis of corneal keratocyte-specific markers ALDH3A1, KERA, LUM and DCN; extracellular matrix markers COL1A1, COL3A1, COL5A1 and myofibroblast marker αSMA (ACTA2) as quantified by rtPCR. Gene expression is normalized to GAPDH (n=3 for all data shown).

in the corneal stroma, were also assessed. They were significantly enhanced by day 28 for 1:1 PCL/SF compared with PCL only. The increased expression of these proteins should lead to improved scaffold deposition, which is vital for tissue formation. There was no significant

change in αSMA (ACTA2) recorded.

4. Discussion

A bioengineered cornea must be transparent, biologically active and cause minimal immunogenic reaction after transplantation. PCL nanofibrous scaffolds have been established as a potential candidate for ocular surface regeneration due to its ability to mimic the ECM of the ocular surface [51]. The present study was conducted to improve the transparency and cytocompatibility of PCL scaffolds for corneal reconstruction by the addition of SF and surface plasma treatment, with the aim of allowing the best environment for quiescent, normal, keratocytes.

The combination of natural and synthetic polymer hybrids through electrospinning offers a scaffold with enhanced properties. However, there is substantial evidence indicating that blend solutions containing more than 30% of one constituent, including the blend system, often exhibit phase separation [52]. This phase separation can lead to inhomogeneities at the ultrastructure level and uncontrollable material properties, which impacts their value in tissue engineering. PCL and SF can be dissolved in chloroform to create miscible solutions. Chloroform acts as a good solvent for PCL and can also dissolve silk protein. However, after being left for 6–8 h, the solution separates into different phases. SF is a polyampholyte protein containing both amino and carboxyl groups. When SF is dissolved in chloroform, its molecules become positively charged due to amino group protonation. The charges between SF molecules repel each other, preventing mutual condensation. However, when SF is blended with PCL to form the SF/PCL dope solution, the protein molecules are exposed to a highly hydrophobic PCL environment. In response to interacting with the PCL molecules, the protein molecules undergo a compact conformation, wrapping their internal hydrophilic groups and exposing their hydrophobic groups [52]. Consequently, the compact SF molecules can adhere together and form larger aggregates. As a result, no phase separation has been observed initially (up to 6–8 h).

The hydrophobicity of PCL restricts cell adherence, so in this study SF was blended with PCL to improve cell attachment as well as introducing other benefits such as improved mechanical strength. To further improve cell attachment and phenotype, a simple plasma treatment was used to enhance the surface properties of the nanofibrous scaffolds. Plasma treatment has been used as an effective and economical method to modify polymeric material's surface for tissue engineering [53,54]. Surface modification of the scaffolds resulted in increased hydrophilicity and enhanced cell proliferation. Changing nanoscale characteristics of the scaffolds is also likely to have induced higher adsorption of adhesive molecules, which is known to improve cell adherence [55].

By increasing hydrophilicity with plasma treatment, there is closer contact of water with the scaffold; this additionally increased light transmission by reducing refraction. The measured RI of nanofibrous scaffold (RI~1.44) is close to that of the human cornea [3]. The improvement in light transmission and the similarities of refraction support the value of a PCL/SF scaffold for engineered stromal constructs.

The similarity between the FTIR spectra of the PCL/SF blends, compared with those of PCL and SF alone, validates the structural stability of the fabricated scaffolds. This may indicate that they will also degrade at the rates of the individual components, which gives opportunity to more readily tune biodegradation. Silk fibroin has remarkable mechanical strength, which is due to the small, oriented, β -sheet crystals in them at nanoscale, as well as the shear-alignment amongst fibre chains [56]. Hence, as expected, the modulus of nanofibrous matrices increased with increasing SF concentration.

The 1:1 PCL/SF blend ratio for both 4 and 6 wt% concentrations of SF was selected for more detailed study of keratocyte cytocompatibility. This confirmed that the cells exhibited a greater affinity toward the plasma-treated PCL/SF surface compared with the plasma-treated PCL alone. This may be due to the addition of SF, which reduced the decreased hydrophobicity. Although fibroin mainly consists of hydrophobic amino acids (e.g., glycine, alanine) the rest of its structure adds hydrophilicity, such as the increasing number of hydrophilic groups

(-NH₂/-CO) with fibroin concentration, which has also been noted for other blended scaffolds [57]. This increase in hydrophilic groups may also explain why the 1:1 blends with 6%SF swelled more quickly than 4%SF.

The results also confirmed that scaffold solely made of PCL resists enzymatic degradation, such that it could be expected to remain for more than a month, whereas adding a SF component reduces resistance and marked degradation has occurred within 3 weeks. The rate of SF enzymatic degradation has been reported (~15wt% weight loss in 12 h) [58] and a shorter timeframe of degradation compared with PCL alone can be beneficial to allow keratocytes to lay down natural scaffold and continue corneal repair. Degradation of silk-based scaffolds using proteinase K and certain typical human enzymes may have similar trends [59]. However, we cannot extrapolate proteinase K degradation study data to the degradation in the human body, as improving the permeability for oxygen and solvents, the increased fibroin content facilitated degradation of blended constructs [60]. Changes of SF manufacture can be tuned to select the most advantageous rate of degradation to optimise repair.

Effective cellular adhesion onto scaffolds requires development of a well-ordered ECM [61] and the presence of organized ECM is necessary for tissue regeneration. The inherent biocompatibility and nano-scaled fibre diameter of SF may explain how adding SF to PCL improves blended scaffolds' cytocompatibility [62]. Initial cell attachment, after 5 hours of seeding, in both PCL/SF blended scaffolds was higher compared to PCL alone. After 21 days of culture, cellular proliferation was also higher for PCL/SF blended scaffolds, compared to PCL. These results appear to indicate that the final cell density was not solely due to differences in initial cell adhesion, the blended scaffolds support both higher initial cell adhesion and also subsequent cell proliferation. In other studies, improved cell adhesion on blended scaffolds provided a more stable and differentiated phenotype of cultured keratocytes compared to control scaffolds [63].

By using conditions to favour a keratocyte-associated phenotype, there was a marked expression of keratocyte-associated markers, as well as corneal ECM specific markers and sGAG quantification that was significantly greater for PCL/SF blended scaffolds, compared to control PCL scaffold. The cytoskeletal organisation induced by the alignment of fibres and presence of SF appear to have contributed to the beneficial gene expression.

5. Conclusion

In this study, step-wise optimization identified a surface-modified PCL/SF nanofibrous scaffold for corneal stromal regeneration. It was shown that of the different compositions investigated, a 1:1 PCL/SF blend fabricated with a 2500-RPM mandrel speed exhibited an aligned, nanoscale fibre diameter that supported cellular proliferation, ECM formation, and keratocyte-associated gene expression. Fibre alignment appeared to affect cell morphology with cells of displaying normal phenotype aligning along the direction of the fibres. Further studies will need to investigate whether longer-term culture will allow the keratocytes to reach a quiescent state, where proliferation minimises and cell density is constant. There is also potential to explore the incorporation of multiple additional regulatory signals, involving growth factors, drugs, and bioactive molecules, towards more effective corneal tissue regeneration therapies.

Author Disclosure Statement

No competing financial interests exist.

Declaration of Competing Interest

The authors declare that they have no known competing financial interests or personal relationships that could have appeared to influence

the work reported in this paper.

Data availability

Data will be made available on request.

Acknowledgments

The research is supported by funding from the European Research Council (ERC) under the European Union's Horizon 2020 research and innovation program (grant agreement no. 637460) and from Science Foundation Ireland (15/ERC/3269).

Supplementary materials

Supplementary material associated with this article can be found, in the online version, at doi:10.1016/j.bbiosy.2023.100083.

References

- Quantock AJ, Young RD. Development of the corneal stroma, and the collagen–proteoglycan associations that help define its structure and function. *Dev Dyn* 2008;237(10):2607–21.
- Fitch JM, Gross J, Mayne R, Johnson-Wint B, Linsenmayer TF. Organization of collagen types I and V in the embryonic chicken cornea: monoclonal antibody studies. *Proc Natl Acad Sci* 1984;81(9):2791–5.
- Maurice DM. The structure and transparency of the cornea. *J Physiol* 1957;136(2): 263.
- Meek KM, Knupp C. Corneal structure and transparency. *Prog Retin Eye Res* 2015; 49:1–16.
- Robaei D, Watson S. Corneal blindness: a global problem. *Clin Experiment Ophthalmol* 2014;42(3):213–4.
- Gain P, Jullienne R, He Z, Aldossary M, Acquart S, Cognasse F, Thuret G. Global survey of corneal transplantation and eye banking. *JAMA Ophthalmol* 2016;134 (2):167–73.
- Lynch AP, Wilson SL, Ahearne M. Dextran preserves native corneal structure during decellularization. *Tissue Eng C Methods* 2016;22(6):561–72.
- Hashimoto Y, Funamoto S, Sasaki S, Honda T, Hattori S, Nam K, Kimura T, et al. Preparation and characterization of decellularized cornea using high-hydrostatic pressurization for corneal tissue engineering. *Biomaterials* 2010;31(14):3941–8.
- Ghezzi CE, Rnjak-Kovacina J, Kaplan DL. Corneal tissue engineering: recent advances and future perspectives. *Tissue Eng B Rev* 2015;21(3):278–87.
- Brunette I, Roberts CJ, Vidal F, Harissi-Dagher M, Lachaine J, Sheardown H, Durr GM, Proulx S, Griffith M. Alternatives to eye bank native tissue for corneal stromal replacement. *Prog Retin Eye Res* 2017;59:97–130.
- Liu W, Merrett K, Griffith M, Fagerholm P, Dravida S, Heyne B, Scaiano JC, et al. Recombinant human collagen for tissue engineered corneal substitutes. *Biomaterials* 2008;29(9):1147–58.
- Ahearne M, Liu KK, Haj AJEL, Then KY, Rau S, Yang Y. Online monitoring of the mechanical behavior of collagen hydrogels: influence of corneal fibroblasts on elastic modulus. *Tissue Eng C Methods* 2010;16(2):319–27.
- Farrugia BL, Lord MS, Whitelock JM, Melrose J. Harnessing chondroitin sulphate in composite scaffolds to direct progenitor and stem cell function for tissue repair. *Biomater Sci* 2018;6(5):947–57.
- Hassell JR, Birk DE. The molecular basis of corneal transparency. *Exp Eye Res* 2010;91(3):326–35.
- Lai JY, Li YT, Cho CH, Yu TC. Nanoscale modification of porous gelatin scaffolds with chondroitin sulfate for corneal stromal tissue engineering. *Int J Nanomed* 2012;7:1101.
- Ahearne M, Lynch AP. Early observation of extracellular matrix-derived hydrogels for corneal stroma regeneration. *Tissue Eng C Methods* 2015;21(10):1059–69.
- Ahearne M, Coyle A. Application of UVA-riboflavin crosslinking to enhance the mechanical properties of extracellular matrix derived hydrogels. *J Mech Behav Biomed Mater* 2016;54:259–67.
- Luo LJ, Lai JY, Chou SF, Hsueh YJ, Ma DHK. Development of gelatin/ascorbic acid cryogels for potential use in corneal stromal tissue engineering. *Acta Bio Mater* 2018;65:123–36.
- Nguyen DD, Yao CH, Luo LJ, Chen HC, Hsueh YJ, Ma DHK, Lai JY. Oxidation-mediated scaffold engineering of hyaluronic acid-based microcarriers enhances corneal stromal regeneration. *Carbohydr Polym* 2022;292:119668.
- Ahearne M, Fernández-Pérez J, Masterton S, Madden PW, Bhattacharjee P. Designing scaffolds for corneal regeneration. *Adv Funct Mater* 2020:1908996.
- Chou SF, Luo LJ, Lai JY, Ma DHK. Role of solvent-mediated carbodiimide cross-linking in fabrication of electrospun gelatin nanofibrous membranes as ophthalmic biomaterials. *Mater Sci Eng C* 2017;71:1145–55.
- Hutmacher DW, Schantz T, Zein I, Ng KW, Hin Teoh S, Tan KC. Mechanical properties and cell cultural response of polycaprolactone scaffolds designed and fabricated via fused deposition modeling. *J Biomed Mater Res* 2001;55(2):203–16. An Official Journal of The Society for Biomaterials, The Japanese Society for Biomaterials, and The Australian Society for Biomaterials and the Korean Society for Biomaterials.
- Lee CH, Li YJ, Huang CC, Lai JY. Poly (ϵ -caprolactone) nanocapsule carriers with sustained drug release: single dose for long-term glaucoma treatment. *Nanoscale* 2017;9(32):11754–64.
- Nguyen DD, Luo LJ, Yang CJ, Lai JY. Highly retina-permeating and long-acting resveratrol/metformin nanotherapeutics for enhanced treatment of macular degeneration. *ACS Nano* 2022;17(1):168–83.
- Bhattacharjee P, Naskar D, Kim HW, Maiti TK, Bhattacharya D, Kundu SC. Non-mulberry silk fibroin grafted PCL nanofibrous scaffold: promising ECM for bone tissue engineering. *Eur Polym J* 2015;71:490–509.
- He L, Chen J, Farson DF, Lannutti JJ, Rokhlin SI. Wettability modification of electrospun poly (ϵ -caprolactone) fibers by femtosecond laser irradiation in different gas atmospheres. *Appl Surf Sci* 2011;257(8):3547–53.
- Ko YG, Kim YH, Park KD, Lee HJ, Lee WK, Park HD, Kim SH, Lee GS, Ahn DJ. Immobilization of poly (ethylene glycol) or its sulfonate onto polymer surfaces by ozone oxidation. *Biomaterials* 2001;22(15):2115–23.
- Uchida E, Uyama Y, Ikada Y. Surface graft polymerization of ionic monomers onto poly (ethylene terephthalate) by UV-irradiation without degassing. *J Appl Polym Sci* 1993;47(3):417–24.
- Ozdemir M, Sadikoglu H. A new and emerging technology: Laser-induced surface modification of polymers. *Trends Food Sci Technol* 1998;9(4):159–67.
- Zhao J, Geuskens G. Surface modification of polymers VI. Thermal and radiochemical grafting of acrylamide on polyethylene and polystyrene. *Eur Polym J* 1999;35(12):2115–23.
- Yoo HS, Kim TG, Park TG. Surface-functionalized electrospun nanofibers for tissue engineering and drug delivery. *Adv Drug Deliv Rev*, 61; 2009. p. 1033–42.
- Ceria A, Hauser PJ. Atmospheric plasma treatment to improve durability of a water and oil repellent finishing for acrylic fabrics. *Surf Coat Technol* 2010;204(9-10): 1535–41.
- Fernández-Pérez J, Kador KE, Lynch AP, Ahearne M. Characterization of extracellular matrix modified poly (ϵ -caprolactone) electrospun scaffolds with differing fiber orientations for corneal stroma regeneration. *Mater Sci Eng C* 2020; 108:110415.
- Tao H, Kaplan DL, Omenetto FG. Silk materials—a road to sustainable high technology. *Adv Mater* 2012;24(21):2824–37.
- Ma D, Wang Y, Dai W. Silk fibroin-based biomaterials for musculoskeletal tissue engineering. *Mater Sci Eng C* 2018;89:456–69.
- Koh LD, Yeo J, Lee YY, Ong Q, Han M, Tee BCK. Advancing the frontiers of silk fibroin protein-based materials for futuristic electronics and clinical wound-healing (invited review). *Mater Sci Eng C* 2018;86:151–72.
- Applegate MB, Partlow BP, Coburn J, Marelli B, Pirie C, Pineda R, Kaplan DL, Omenetto FG. Photocrosslinking of silk fibroin using riboflavin for ocular prostheses. *Adv Mater* 2016;28(12):2417–20.
- Wang S, Ghezzi CE, Gomes R, Pollard RE, Funderburgh JL, Kaplan DL. *In vitro* 3D corneal tissue model with epithelium, stroma, and innervation. *Biomaterials* 2017; 112:1–9.
- Lawrence BD, Marchant JK, Pindrus MA, Omenetto FG, Kaplan DL. Silk film biomaterials for cornea tissue engineering. *Biomaterials* 2009;30(7):1299–308.
- Bray LJ, George KA, Ainscough SL, Hutmacher DW, Chirila TV, Harkin DG. Human corneal epithelial equivalents constructed on Bombyx mori silk fibroin membranes. *Biomaterials* 2011;32(22):5086–91.
- Wu J, Rnjak-Kovacina J, Du Y, Funderburgh ML, Kaplan DL, Funderburgh JL. Corneal stromal bioequivalents secreted on patterned silk substrates. *Biomaterials* 2014;35(12):3744–55.
- Madden PW, Klyubin I, Ahearne MJ. Silk fibroin safety in the eye: a review that highlights a concern. *BMJ Open Ophthalmol* 2020;5(1):e000510.
- Puerta M, Arango MC, Jaramillo-Quiceno N, Álvarez-López C, Restrepo-Osorio A. Influence of ethanol post-treatments on the properties of silk protein materials. *SN Appl Sci* 2019;1(11):1–7.
- Bhattacharjee P, Kundu B, Naskar D, Kim HW, Bhattacharya D, Maiti TK, Kundu SC. Potential of inherent RGD containing silk fibroin–poly (ϵ -caprolactone) nanofibrous matrix for bone tissue engineering. *Cell Tissue Res* 2016;363:525–40.
- Robinson AJ, Pérez-Nava A, Ali SC, Betzabe González-Campos J, Holloway JL, Cosgriff-Hernandez EM. Comparative analysis of fiber alignment methods in electrospinning. *Matter* 2021;4(3):821–44.
- Hotaling NA, Bharti K, Kriel H, Jr CGS. DiameterJ: A validated open source nanofiber diameter measurement tool. *Biomaterials* 2015;61:327–38.
- Lynch AP, O'Sullivan F, Ahearne M. The effect of growth factor supplementation on corneal stromal cell phenotype *in vitro* using a serum-free media. *Exp Eye Res* 2016;151:26–37.
- Yoshida S, Shimamura S, Shimazaki J, Shinozaki N, Tsubota K. Serum-free spheroid culture of mouse corneal keratocytes. *Invest Ophthalmol Vis Sci* 2005;46(5): 1653–8.
- Chin L.J., and S. Uematsu. "Biodegradation of polymeric systems." *Nanocomposites with Biodegradable Polymers: Synthesis, Properties, and Future Perspectives* 68 (2011): 28.
- Bhattacharjee P, Fernández-Pérez J, Ahearne M. Potential for combined delivery of riboflavin and all-trans retinoic acid, from silk fibroin for corneal bioengineering. *Mater Sci Eng C* 2019;105:110093.
- Sharma S, Mohanty S, Gupta D, Jassal M, Agrawal AK, Tandon R. Cellular response of limbal epithelial cells on electrospun poly- ϵ -caprolactone nanofibrous scaffolds for ocular surface bioengineering: a preliminary *in vitro* study. *Mol Vis* 2011;17: 2898.

- [52] Zhu J, Luo J, Zhao X, Gao J, Xiong J. Electrospun homogeneous silk fibroin/poly (ϵ -caprolactone) nanofibrous scaffolds by addition of acetic acid for tissue engineering. *J Biomater Appl* 2016;31(3):421–37.
- [53] Greene G, Yao G, Tannenbaum R. Wetting characteristics of plasma-modified porous polyethylene. *Langmuir* 2003;19(14):5869–74.
- [54] Sharma S, Gupta D, Mohanty S, Jassal M, Agrawal AK, Tandon R. Surface-modified electrospun poly (ϵ -caprolactone) scaffold with improved optical transparency and bioactivity for damaged ocular surface reconstruction. *Invest Ophthalmol Vis Sci* 2014;55(2):899–907.
- [55] Chua KN, Chai C, Lee PC, Tang YN, Ramakrishna S, Leong KW, Mao HQ. Surface-aminated electrospun nanofibers enhance adhesion and expansion of human umbilical cord blood hematopoietic stem/progenitor cells. *Biomaterials* 2006;27(36):6043–51.
- [56] Altman GH, Diaz F, Jakuba C, Calabro T, Horan RL, Chen J, Lu H, Richmond J, Kaplan DL. Silk-based biomaterials. *Biomaterials* 2003;24(3):401–16.
- [57] Lim JS, Ki CS, Kim JW, Lee KG, Kang SW, Kweon HY, Park YH. Fabrication and evaluation of poly (ϵ -caprolactone)/silk fibroin blend nanofibrous scaffold. *Biopolymers* 2012;97(5):265–75.
- [58] Jin HJ, Park J, Karageorgiou V, Kim UJ, Valluzzi R, Cebe P, Kaplan DL. Water-stable silk films with reduced β -sheet content. *Adv Funct Mater* 2005;15(8):1241–7.
- [59] Li M, Ogiso M, Minoura N. Enzymatic degradation behavior of porous silk fibroin sheets. *Biomaterials* 2003;24(2):357–65.
- [60] Kuchaiyaphum P, Punyodom W, Watanesk S, Watanesk R. Composition optimization of polyvinyl alcohol/rice starch/silk fibroin-blended films for improving its eco-friendly packaging properties. *J Appl Polym Sci* 2013;129(5):2614–20.
- [61] Verma S, Kumar N. Effect of biomimetic 3D environment of an injectable polymeric scaffold on MG-63 osteoblastic-cell response. *Mater Sci Eng C* 2010;30(8):1118–28.
- [62] Binulal NS, Deepthy M, Selvamurugan N, Shalumon KT, Suja S, Mony U, Jayakumar R, Nair SV. Role of nanofibrous poly (ϵ -caprolactone) scaffolds in human mesenchymal stem cell attachment and spreading for *in vitro* bone tissue engineering—response to osteogenic regulators. *Tissue Eng Part A* 2010;16(2):393–404.
- [63] Watt FM. Effect of seeding density on stability of the differentiated phenotype of pig articular chondrocytes in culture. *J Cell Sci* 1988;89(3):373–8.